The Plant Cell, Vol. 27: 1218–1227, April 2015, www.plantcell.org

Identification and Characterization of a Golgi-Localized UDP-Xylose Transporter Family from Arabidopsis[OPEN]

Berit Ebert,[a,b,c,1] Carsten Rautengarten,[a,c,1] Xiaoyuan Guo,[b] Guangyan Xiong,[d] Solomon Stonebloom,[a] Andreia M. Smith-Moritz,[a] Thomas Herter,[a] Leanne Jade G. Chan,[a] Paul D. Adams,[a,e] Christopher J. Petzold,[a] Markus Pauly,[d] William G.T. Willats,[b] Joshua L. Heazlewood,[a,c] and Henrik Vibe Scheller[a,d,2]

[a] Joint BioEnergy Institute and Physical Biosciences Division, Lawrence Berkeley National Laboratory, Berkeley, California 94720
[b] Department of Plant and Environmental Sciences, Faculty of Science, University of Copenhagen, C 1871 Copenhagen, Denmark
[c] ARC Centre of Excellence in Plant Cell Walls, School of BioSciences, The University of Melbourne, Victoria 3010, Australia
[d] Department of Plant and Microbial Biology, University of California, Berkeley, California 94720
[e] Department of Bioengineering, University of California, Berkeley, California 94720

Most glycosylation reactions require activated glycosyl donors in the form of nucleotide sugars to drive processes such as posttranslational modifications and polysaccharide biosynthesis. Most plant cell wall polysaccharides are biosynthesized in the Golgi apparatus from cytosolic-derived nucleotide sugars, which are actively transferred into the Golgi lumen by nucleotide sugar transporters (NSTs). An exception is UDP-xylose, which is biosynthesized in both the cytosol and the Golgi lumen by a family of UDP-xylose synthases. The NST-based transport of UDP-xylose into the Golgi lumen would appear to be redundant. However, employing a recently developed approach, we identified three UDP-xylose transporters in the *Arabidopsis thaliana* NST family and designated them UDP-XYLOSE TRANSPORTER1 (UXT1) to UXT3. All three transporters localize to the Golgi apparatus, and UXT1 also localizes to the endoplasmic reticulum. Mutants in *UXT1* exhibit ~30% reduction in xylose in stem cell walls. These findings support the importance of the cytosolic UDP-xylose pool and UDP-xylose transporters in cell wall biosynthesis.

INTRODUCTION

Plant cell walls are composed of various polysaccharides and with the exception of cellulose and callose, these cell wall polysaccharides are biosynthesized in the lumen of the Golgi apparatus by families of glycosyltransferases (Scheible and Pauly, 2004; Liepman et al., 2010). The nucleotide sugar substrates essential for the biosynthesis of these polysaccharides are predominantly made in the cytosol. To overcome the subcellular partitioning of substrates and enzymes, nucleotide sugar transporters (NSTs) have evolved to allow the transport of nucleotide sugars from the cytosol into the Golgi and endoplasmic reticulum (ER) lumen. NSTs belong to the NST/triose phosphate translocator (TPT) superfamily, and the fact that they are present in all eukaryotes testifies to their biological significance (Knappe et al., 2003). Phylogenetic analyses have identified more than 50 members in *Arabidopsis thaliana* that are distributed in six clades (Rautengarten et al., 2014). However, functional characterization of members of the NST family at the molecular level has progressed slowly. In the past decade, only a few NSTs have been characterized, thus far accounting for the transport of GDP-mannose (GDP-Man), UDP-galactose (UDP-Gal), UDP-glucose (UDP-Glc), and CMP-sialic acid, although sialic acid has not been found in plants (Baldwin et al., 2001; Norambuena et al., 2002, 2005; Handford et al., 2004, 2012; Bakker et al., 2005, 2008; Rollwitz et al., 2006; Zhang et al., 2011; Mortimer et al., 2013). Recently, we developed a biochemical approach that allows the rapid and reliable determination of NST activities and led to the identification and characterization of the Arabidopsis bifunctional UDP-rhamnose (UDP-Rha)/UDP-Gal transporter (URGT) clade (Rautengarten et al., 2014).

Xyl is a key component of various plant cell wall polymers, including xylan and xyloglucan, which are two of the most abundant cell wall polysaccharides in plants (Ebringerová and Heinze, 2000; Scheller and Ulvskov, 2010). While glucuronoxylan is a major hemicellulose in secondary cell walls, xyloglucan is the major component of the hemicellullosic fraction of primary walls of dicot plants. Minor amounts of Xyl can also be found in pectic polysaccharides, such as rhamnogalacturonan-II and xylogalacturonan (Jensen et al., 2008; Atmodjo et al., 2013), glycoproteins (Strasser et al., 2000), and diverse metabolites. Xylans in vascular plants are mainly composed of a backbone of β-(1,4)-linked xylopyranosyl residues, which may be decorated at *O*-2 or *O*-3 with arabinofuranosyl residues or at *O*-2 with glucuronosyl and 4-*O*-methylglucuronosyl residues to form arabinoxylan found in grasses and glucuronoxylan, the main xylan found in dicots (Tan et al., 2013; Rennie and Scheller, 2014). UDP-Xyl, the activated sugar donor for xylosyltransferases, is biosynthesized via decarboxylation of UDP-glucuronic acid by UDP-XYLOSE SYNTHASE (UXS) (Harper and Bar-Peled, 2002). While most nucleotide sugars are made in the cytosol and require transport into the Golgi lumen, in plants, members of the UXS family have been localized to both the Golgi and cytosolic fractions (Harper and Bar-Peled,

[1] These authors contributed equally to this work.
[2] Address correspondence to hscheller@lbl.gov.
The authors responsible for distribution of materials integral to the findings presented in this article in accordance with the policy described in the Instructions for Authors (www.plantcell.org) are: Joshua L. Heazlewood (Joshua.heazlewood@unimelb.edu.au) and Henrik Vibe Scheller (hscheller@lbl.gov).
[OPEN]Articles can be viewed online without a subscription.
www.plantcell.org/cgi/doi/10.1105/tpc.114.133827

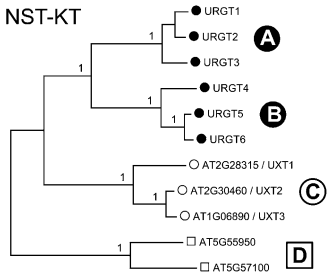

Figure 1. Phylogenetic Tree of the Arabidopsis NST-KT Subfamily.

The full-length amino acid sequences of the Arabidopsis NST-KT subfamily (Knappe et al., 2003) were aligned with Clustal Omega and the tree generated using MEGA6. Numbers at the nodes indicate bootstrap values calculated for 1000 replicates. Subclades were assigned as previously reported (Rautengarten et al., 2014).

2002; Pattathil et al., 2005). Furthermore, UDP-Xyl can also be biosynthesized in the cytosol by a related gene family that also produces UDP-apiose, namely, UDP-API SYNTHASE/UDP-XYL SYNTHASE (Mølhøj et al., 2003). Thus, in plants there seem to be three distinct pathways for UDP-Xyl biosynthesis (Bar-Peled and O'Neill, 2011).

The biosynthesis of UDP-Xyl in the Golgi lumen would argue against the requirement for a UDP-Xyl-specific transporter residing in the Golgi membrane for the biosynthesis of Xyl-containing polysaccharides and glycoproteins. Nevertheless, we obtained evidence that Golgi-localized UDP-Xyl specific transporters exist in Arabidopsis and that at least one Golgi-localized UDP-Xyl transporter is necessary for proper biosynthesis of Xyl-containing cell wall polysaccharides. We designated the three members of this gene family as *UDP-XYL TRANSPORTER1* (*UXT1*) to *UXT3*.

RESULTS

The NST-KT Clade of the Arabidopsis NST/TPT Family

The previously classified NST-KT subfamily is characterized by a highly conserved lysine/threonine (KT) motif (Knappe et al., 2003) and forms clade I of the NST/TPT family (Rautengarten et al., 2014) encompassing 11 putative NSTs (Figure 1). Collectively, they share 25 to 93% identity in their amino acid sequences and include the recently identified URGTs that form subclades (A) and (B) of the NST-KT subfamily (Rautengarten et al., 2014). Another subclade (C) contains three additional members, namely, UXT1 (AT2G28315), UXT2 (AT2G30460), and UXT3 (AT1G06890). UXT1 shares 66% and 67% identity with UXT2 and UXT3, respectively. UXT2 and UXT3 share 92% identity in their amino acid sequences. Members of the uncharacterized subclade (D) share 25 to 28% identity in their amino acid sequences when compared with all other members of the NST-KT family (Rautengarten et al., 2014).

UXTs Are Ubiquitously Expressed and Localized to the Golgi Apparatus

Publicly available microarray expression data comprising the AtGenExpress Developmental Data Set (Schmid et al., 2005) have shown ubiquitous expression for *UXT2* and *UXT3* throughout plant development, with *UXT3* showing highest expression in pollen and flowers. Since *UXT1* is not present on the Affymetrix ATH1 array, we assessed the relative expression levels using quantitative RT-PCR (Figure 2A). Expression data obtained by quantitative RT-PCR for *UXT2* and *UXT3* are consistent with the microarray expression data, confirming ubiquitous but relatively low expression for both genes. *UXT1* is more highly expressed in most tissues analyzed, with some variation in expression, especially in the stem tissue. To determine the subcellular localization

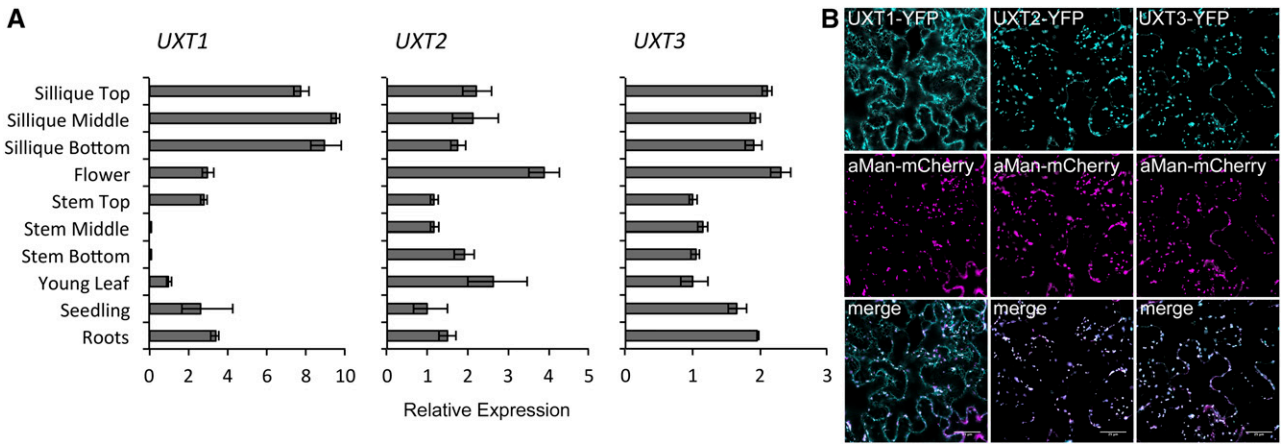

Figure 2. Expression Pattern and Subcellular Localizations of UXTs.

(A) Quantitative RT-PCR of *UXT* expression in Arabidopsis organs and developmental stages. The three *UXT*s are expressed throughout the plant with *UXT1* showing the highest expression levels. Expression levels are mean ± SD (n = 3) technical replicates relative to the reference genes.
(B) Subcellular localization of the UXTs. C-terminal YFP fusions were transiently coexpressed with the α-mannosidase I Golgi marker in *N. benthamiana* leaves. All three UXTs colocalize with the Golgi marker. UXT1 also colocalizes with an ER marker (Supplemental Figure 1). Bar = 25 μm.

of the UXTs, we generated C-terminal yellow fluorescent protein (YFP) fusions of the coding sequences and expressed them transiently in *Nicotiana benthamiana* leaves. All three UXTs localized to Golgi-like punctate structures and colocalized with the Golgi-marker α-mannosidase I, supporting their function as Golgi NSTs (Figure 2B). In contrast to UXT2 and UXT3, UXT1 also appeared to be localized to the ER and colocalized with the ER marker ER-ck (Nelson et al., 2007) (Supplemental Figure 1).

Determining the in Vitro Functions of the Arabidopsis UXTs

To assess the function of the UXTs, each was heterologously expressed in *Saccharomyces cerevisiae* (yeast) and microsomal proteins were prepared. Immunoblot analysis confirmed the presence of the specific UXT proteins in yeast microsomal extracts (Figure 3A). Subsequently, microsomal proteins were reconstituted into liposomes for transport assays. Proteoliposomes preloaded with either UMP, GMP, CMP, or AMP were incubated with a mixture of 16 nucleotides/nucleotide sugars (Figure 3B). Non-transported substrates were removed by gel filtration, and the content of the liposomes was analyzed by liquid chromatography-tandem mass spectrometry (LC-MS/MS). The LC-MS/MS analysis of nucleotide sugars after transport by UXTs could be readily assessed when compared with the empty vector control (Figures 3C and 3D). All three UXTs had the capacity to transport UDP-Xyl as well as minor amounts of UDP-arabinopyranose (UDP-Ara*p*) in vitro when the proteoliposomes were preloaded with UMP (Figure 3E). By contrast, when proteoliposomes were preloaded with GMP, only transport of GDP-sugars was observed (Figure 3F), resulting from endogenous activity present in yeast microsomal preparations, since the incorporation levels were similar to those observed in control reactions (yeast transformed with the empty vector). No significant transport activities were observed when proteoliposomes were preloaded with AMP or CMP.

The UXT-mediated transport of UDP-Xyl was saturable in a concentration and time-dependent manner (Figures 4A and 4B). To determine K_{cat}, we measured the amount of UXT protein in the proteoliposomes using multiple reaction monitoring (MRM) mass spectrometry as explained in Methods and Supplemental Table 1. The analysis of the UXTs revealed apparent K_m values for UDP-Xyl in the range of 40 to 60 μM with turnover rates of 3 to 12 s^{-1} (Table 1). As previously determined, the UDP-Xyl content in various Arabidopsis organs is in the range of 40 to 120 pmol mg^{-1} dry weight (Rautengarten et al., 2014). Considering the volume of the central vacuole in plants, these measurements indicate that the cellular levels of UDP-Xyl are in the micromolar range. Thus, we estimate that the affinity constants (K_m) for all three UXTs are within physiological range. By contrast, estimations of the K_m for UDP-Ara*p*, which was transported by all three UXTs to a lower extent, revealed values of ≥200 μM, which would be inconsistent with endogenous concentrations. UDP-Ara*p* concentrations in Arabidopsis organs are very similar to UDP-Xyl concentrations

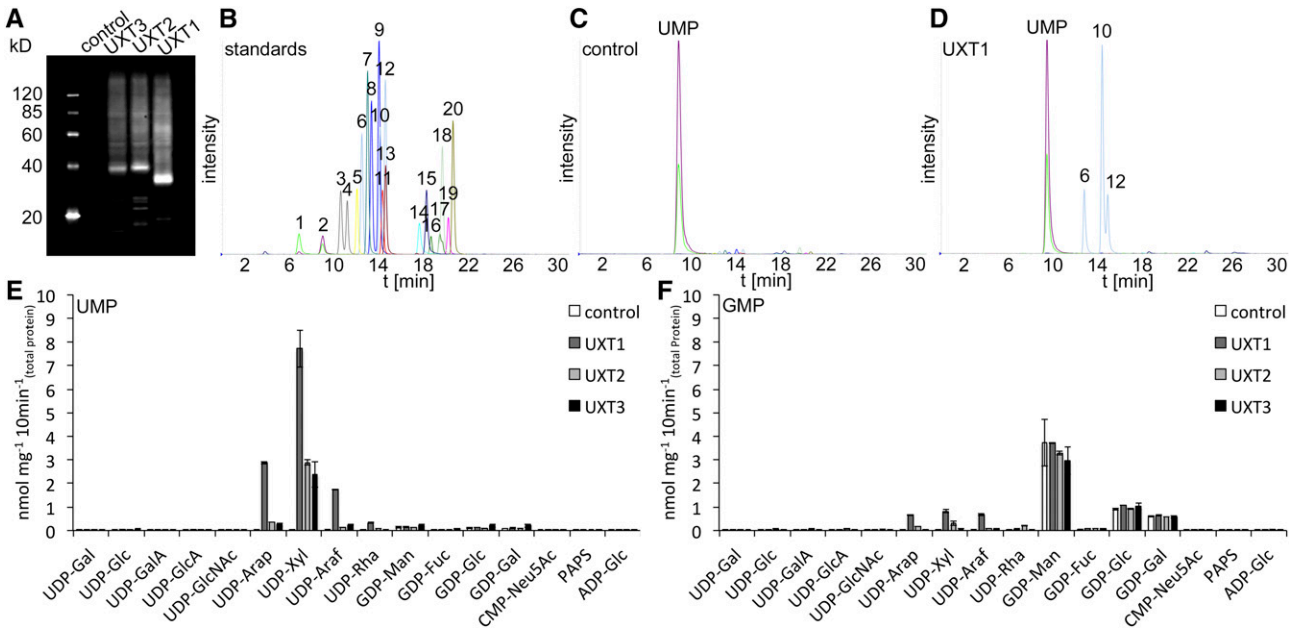

Figure 3. LC-MS/MS Analysis of NST Activities of UXTs.

(A) Immunoblot analysis of UXT expression in yeast microsomal protein extracts (2.5 μg), including the empty vector control.

(B) Separation of a 20 nucleotide/nucleotide sugar mix: 1, CMP; 2, UMP; 3, UDP-GalA; 4, UDP-glucuronic acid; 5, CMP-sialic acid; 6, UDP-Ara*p*; 7, UDP-Rha; 8, UDP-Gal; 9, UDP-Glc; 10, UDP-Xyl; 11, UDP-GlcNAc/GalNAc; 12, UDP-Ara*f*; 13, adenosine 3′-phosphate 5′ phosphosulfate; 14, GMP; 15, AMP; 16, GDP-Man; 17, GDP-Gal; 18, GDP-Glc, 19, GDP-Fuc; and 20, ADP-Glc.

(C) and **(D)** Reconstitution of empty vector control **(C)** and UXT1 **(D)** into liposomes and analysis by LC-MS/MS after simultaneous incubation with 16 nucleotide sugar substrates.

(E) and **(F)** Quantification of nucleotide sugar uptake of proteoliposomes containing UXT1 and preloaded with UMP **(E)** and GMP **(F)**. Data represent the mean and SD of $n = 2$ independent experiments.

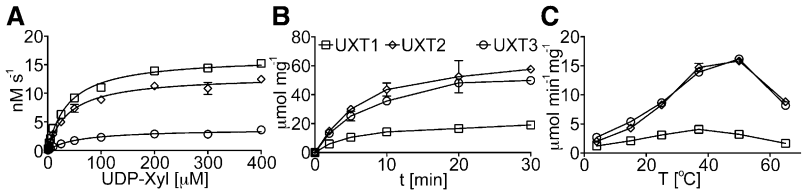

Figure 4. Time- and Temperature-Dependent Transport Activities of the Arabidopsis UXTs.

(A) Proteoliposomes, preloaded with UMP, were incubated with UDP-Xyl at varying concentration (0.5 to 400 μM) for 2 min at 25°C.
(B) and **(C)** Proteoliposomes were incubated with UDP-Xyl at a concentration of 50 μM for the indicated time points at 25°C, or varying temperatures. Values are normalized to the actual NST content present in the proteoliposome preparations. Data represent the mean and SD of $n = 2$ independent experiments.

(Rautengarten et al., 2014); hence, the high affinity constants or K_m values indicate that the UXTs are most likely not significantly involved in UDP-Ara*p* transport in vivo. The temperature optimums for transport of UDP-Xyl for the three UXTs ranged from 37 to 55°C (Figure 4C).

The Role of the UXTs in Planta

To evaluate the in vivo function of the UXTs, we obtained homozygous T-DNA lines. Two independent lines were acquired for *UXT1*, and single insertion lines were identified for *UXT2* and *UXT3*. Finally, a double knockout was generated between *uxt2* and *uxt3*, and the absence of respective full-length transcripts was confirmed by PCR (Supplemental Figure 2).

To assess if mutations in the UXTs affect the biosynthesis of specific polysaccharides, we prepared alcohol insoluble residue (AIR) from leaves, flowers, and young (upper) and mature (lower) inflorescence stem tissue from 6- to 8-week-old plants and analyzed the monosaccharide composition (Supplemental Table 2). Flowers and leaves showed no significant differences in the monosaccharide composition between any of the mutants and Columbia-0 (Col-0; $P > 0.05$, ANOVA and Duncan's test for multiple comparisons). Stem data showed a significant difference in the monosaccharide composition of *uxt1-1* and *uxt1-2* compared with Col-0 ($P < 0.05$), whereas the other mutants did not show a difference from Col-0. In *uxt1-1* and *uxt1-2*, only Xyl and glucuronic acid (GlcA) were significantly decreased in stems compared with Col-0 (Figures 5A and 5B). The Xyl content in mature inflorescence stems from the *uxt1* mutants was decreased by 16% (Figure 5B), whereas a reduction of 34% was observed in young stem tissue (Figure 5A). These data confirm the importance of UXT1 for the biosynthesis of Xyl-containing cell wall polymers. In addition, a significant reduction in cell wall GlcA content of ~25 to 37% was observed in mature and young parts of the inflorescence stems from *uxt1* mutants. Since the monosaccharide compositions are relative measurements, the decrease in Xyl and GlcA was accompanied by an apparent increase in other monosaccharides. However, the ratio between the other sugars was not significantly changed in any of the samples, indicating that a loss of function of UXT1 had no direct effect on any sugars besides Xyl and GlcA. Notably, while GlcA content was decreased in the mutant, there was no change in the 4-*O*-methyl ether (MeGlcA) content, i.e., the ratio between the methylated and nonmethylated form of GlcA was much higher in the mutant than in the wild type (Supplemental Figure 3). However, even though there was a significant reduction of Xyl and GlcA in the *uxt1* mutants, the plants did not exhibit a morphological phenotype compared with wild-type plants.

Cell Wall Profiling of the *uxt1* Mutants

To analyze the changes in the cell wall composition of *uxt1* mutants in more detail, we performed comprehensive microarray polymer profiling (CoMPP) analysis on mature (lower) stem material. Cell wall matrix polymers were extracted, spotted onto nitrocellulose membranes to generate microarrays, and probed with a number of different antibodies with specificity for epitopes borne on cell wall polymers (Figure 5C). Since we observed a significant decrease in cell wall xylose in the *uxt1* mutants, we focused specifically on antibodies recognizing xylan structures, including LM10/LM11 (which bind unsubstituted xylans), UX1 (which recognizes GlcA or MeGlcA substitutions on xylan), and AX1 [which was produced against arabinose-substituted β-(1,4)-xylan from wheat (*Triticum aestivum*)]. Clear differences were observed between the *uxt1-1* and *uxt1-2* mutants and the wild type (Figure 5C). Collectively, these probes revealed an apparent reduction in the xylan content and, more specifically, as indicated in the results for the UX1 antibody, in the glucuronoxylan content in *UXT1* mutants when compared with the wild type (Figure 5C). Concomitant with the reduction in xylan content, the results from the CoMPP analysis indicate that other polymers, such as cellulose (recognized by the carbohydrate bonding module CBM3a) and xyloglucan (recognized by antibody LM25), were only slightly affected in *UXT1* mutants. By contrast, results obtained with the LM3 antibody, which recognizes glycan moieties on extensins, indicated that these proteoglycans are enriched in *UXT1* mutants. In addition, oligosaccharide mass profiling (OLIMP) revealed no significant differences in the xyloglucan structure in *uxt1* cell wall preparations compared with the wild type (Table 2).

Table 1. Kinetic Parameters of UDP-Xyl Transport into Proteoliposomes

Parameter	UXT1	UXT2	UXT3
K_m (μM)	39 (3)	40 (4)	58 (9)
V_{max} (nM s^{-1})	16 (0)	13 (0)	4 (0)
K_{cat} (s^{-1})	3.6	10.3	11.7

For each UXT, 20 data points with varying substrate concentrations (0.5 to 400 μM) were acquired. Standard errors are in parentheses.

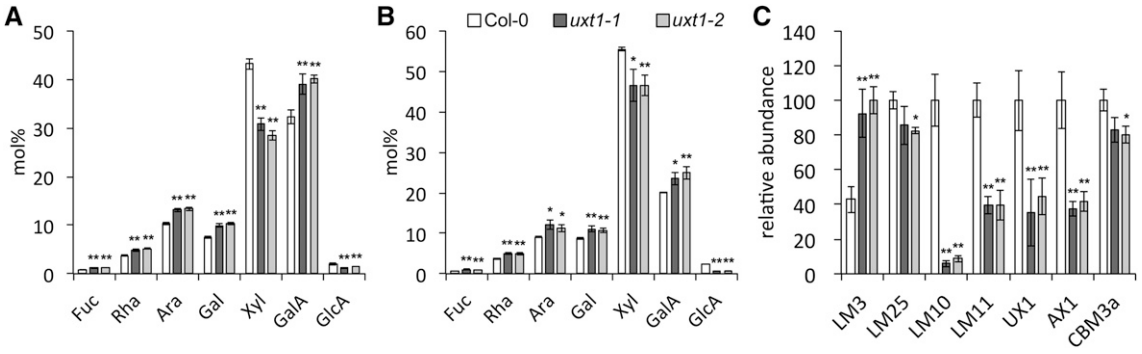

Figure 5. Cell Wall Analysis of *UXT1* Mutants.

(A) and **(B)** Monosaccharide composition of total cell wall extracts from upper **(A)** and lower **(B)** parts of the inflorescence stem. Data represent 10 pooled individuals and mean and SD from six technical replicates. Values are expressed in mol %.

(C) CoMPP analysis with relative abundance of cell wall glycan epitopes. Mean and SD for spot signals (MSS) were obtained by probing microarrays with antibodies (*x* axis) from four technical replicates and the highest MSS set to 100 and all other values adjusted accordingly. For all data, values significantly different from the wild type are marked with asterisks (*P < 0.05 and **P < 0.01; *t* test).

In Arabidopsis, xylan is comprised of domains that differ in their pattern of MeGlcA substitution and is generated by two glucuronosyltransferases, GUX1 and GUX2. The GUX1 enzyme is responsible for the addition of GlcA only to evenly spaced Xyl residues, whereas GUX2 decorates both even and odd spaced Xyl residues (Bromley et al., 2013). To determine if mutations in UXT1 preferentially affect one of the domains, we digested xylan from the *uxt1* mutants and the wild type with the glucuronoxylanase C (XynC) and analyzed the released oligosaccharides by high-performance anion exchange chromatography (HPAEC; Supplemental Figure 4). The xylooligosaccharide profile from the *uxt1* mutants is similar to the profile observed for the wild type, and differences detected in the chromatograms are consistent with the increased ratio of the methylated and nonmethylated form of GlcA in the mutant compared with the wild type (Supplemental Figure 3). However, the pattern of xylan substitution is clearly different from those observed for the *gux1* and *gux2* mutants, thus indicating that UXT1 does not play a role in defining the domain pattern of decoration. Compared with the wild type, the profile from the *uxt1* mutants showed a slight shift toward shorter oligosaccharides, indicating a higher degree of substitution (Supplemental Figure 3).

Since UXT1 localizes to both the Golgi apparatus and the ER, it is possible that UXT1 could also play a role in protein glycosylation. To investigate this in more detail, we analyzed total protein from *UXT* mutants with antibodies against plant *N*-glycan xylosyl and fucosyl epitopes. However, no obvious differences in the *N*-glycan xylosylation pattern of the *UXT* mutants compared with the wild type could be observed. The same was true for the fucosylation pattern, which we analyzed as a control (Supplemental Figure 5). Hence, our results indicate that the UXTs do not have an obvious effect on protein *N*-glycosylation.

DISCUSSION

The majority of nucleotide sugars are actively transported into the Golgi and ER lumen by NSTs (Bar-Peled and O'Neill, 2011). Here, we present evidence for the existence of a Golgi UDP-Xyl transporter family in plants. We identified three previously uncharacterized Arabidopsis NSTs comprising the NST-KT family subclade C. All three members are capable of transporting UDP-Xyl and to a lower extent UDP-Ara*p* in vitro (Figure 4). However, estimations of the K_m values for UDP-Ara*p* indicate that these UXTs are unlikely to transport UDP-Ara*p* in vivo, whereas determined K_m values for UDP-Xyl transport are within the physiological range (Rautengarten et al., 2014).

Analysis of the subcellular localization of the UXTs showed that all three are located in the Golgi apparatus and that UXT1 also

Table 2. Xyloglucan Structure Determined by Oligosaccharide Mass Profiling

Tissue	Plant Line	GXXG (953 *m/z*)	XXXG (1085 *m/z*)	XXLG/XLXG (1247 *m/z*)	XXLG/XLXG +OAc (1289 *m/z*)	XXFG (1393 *m/z*)	XXFG +OAc (1435 *m/z*)	XLFG (1555 *m/z*)	XLFG +OAc (1597 *m/z*)
Lower	Col-0	2.0 ± 0.2	32.5 ± 2.8	9.3 ± 0.7	1.8 ± 0.2	15.0 ± 0.9	14.1 ± 0.8	13.7 ± 1.6	11.5 ± 0.5
Stem	*uxt1-1*	2.1 ± 0.3	33.2 ± 1.8	8.6 ± 0.6	1.4 ± 0.1	16.1 ± 0.5	14.1 ± 0.4	14.3 ± 1.1	10.3 ± 1.0
	uxt1-2	2.1 ± 0.1	35.0 ± 1.3	7.8 ± 0.2	1.4 ± 0.1	15.2 ± 0.2	14.4 ± 0.4	13.3 ± 0.3	10.9 ± 0.9
Upper	Col-0	3.2 ± 0.5	37.5 ± 0.9	13.0 ± 0.2	1.0 ± 0.1	19.0 ± 1.3	7.3 ± 0.3	15.5 ± 0.3	3.5 ± 0.3
Stem	*uxt1-1*	2.7 ± 0.1	33.8 ± 0.7	12.1 ± 0.7	1.2 ± 0.1	20.7 ± 0.9	8.6 ± 1.1	16.1 ± 0.8	4.8 ± 0.2
	uxt1-2	2.9 ± 0.2	36.1 ± 1.4	12.4 ± 0.7	1.4 ± 0.1	20.1 ± 1.2	7.7 ± 0.5	15.0 ± 0.4	4.4 ± 0.3

Relative abundance of xyloglucan oligosaccharides in the upper and lower stem walls was determined by OLIMP. No significant differences (P < 0.05) were observed between the wild type and mutants. Data represent the mean (±SE) of *n* = 3 independent biological replicates. The mass-to-charge ratio (*m/z*) is provided for each oligosaccharide; for nomenclature of the oligosaccharides, see Fry et al. (1993).

localized to the ER, which could indicate a distinct functional role for UXT1. However, we are not aware of any xylosyltransferase reaction that is known to take place in the ER. Although protein *N*-glycosylation is initiated in the ER, the xylosylation has been shown to occur in the Golgi apparatus (Fitchette-lainé et al., 1994; Egelund et al., 2006). Therefore, the possible biological significance of the partial localization of UXT1 to the ER remains unclear. By contrast, the localization to the Golgi apparatus of all three transporters is consistent with the biosynthesis of Xyl-containing glycans in this compartment. The three *UXTs* are expressed throughout plant development. Compared with *UXT1*, *UXT2* and *UXT3* have lower overall expression levels in the tissues analyzed. The *UXT1* transcript varies more substantially, especially in mature stem material where relative expression was lowest but still detectable.

To determine the functions of the UXTs in planta, we identified and analyzed loss-of-function mutants in all three transporters. Neither the *uxt2* nor the *uxt3* mutants exhibited any changes in cell wall monosaccharide composition. This could be due to the lower relative levels of expression for these two genes when compared with *UXT1*. Similarly, the *uxt2 uxt3* double mutants did not show any discernable phenotype, indicating possible minor roles for these genes. Due to the genetic linkage between *UXT1* and *UXT2*, we have not been able to generate a triple homozygous mutant line.

Only *UXT1* mutants showed a significant decrease in cell wall-derived Xyl. This decrease was exclusive to stem material and was more pronounced in material isolated from younger parts of inflorescence stems. This difference based on stem maturity can be explained by the fact that in the developing stem, active cell wall biosynthesis and xylan production is occurring, whereas in mature stem tissue the function of the UDP-Xyl transporter may no longer be needed. Together with the decrease in Xyl in stems, we also observed a proportional reduction in GlcA content. Most of the GlcA in stem cell walls originates from glucuronoxylan; therefore, the proportional reduction in GlcA content is consistent with the suggestion that UXT1 functions predominantly in the biosynthesis of glucuronoxylans. However, the methylated GlcA content remained unchanged in *uxt1* mutant plants when compared with the wild type (Supplemental Figure 3). This observation is consistent with previously published data on xylan mutants, such as *irx8*, *irx9*, and *fra8*, in which the ratio of GlcA to MeGlcA is lower and methylated GlcA predominates (Liepman et al., 2010). Xylooligosaccharide profiling indicated that UXT1 affects both GUX1-dependent and GUX2-dependent xylan domains.

A more detailed characterization of *uxt1* mutants using CoMPP and OLIMP techniques also indicated the importance of UXT1 in glucuronoxylan biosynthesis and revealed that it has little effect on xyloglucan biosynthesis. The latter could be explained by a lower requirement for UDP-Xyl for decoration of matrix polysaccharides, such as xyloglucan and xylogalacturonan, or could hint at a role for the endogenously biosynthesized luminal pool of UDP-Xyl. These findings suggest that UXT1 may be involved in protein interactions with specific glycosyltransferases and associated enzymes involved in biosynthesis of xylan.

The lack of an obvious mutant phenotype for *UXT2* and *UXT3* could indicate that they are not specifically involved in a functional protein complex and may play a generic role in the delivery of cytosolic-derived UDP-Xyl into the Golgi lumen. Interestingly, the URGT1 transporter of UDP-Rha/UDP-Gal also showed a differential role in biosynthesis of different polysaccharides in vivo (Rautengarten et al., 2014). Loss-of-function mutants and overexpressors of *URGT1* showed large changes in content of pectic galactan but no change in the galactose substitutions of xyloglucan. While these observations could suggest substrate channeling in the case of URGT1 and UXT1, it is also possible that differences in K_m values for different glycosyltransferases or different sub-Golgi localizations can explain the apparent specificity.

Both β-(1,4)-xylan synthase and β-(1,4)-galactan synthase are enzymes that make a homopolymer and are nonprocessive enzymes in vitro, i.e., the product profiles indicate that the product is released from the enzyme after each round of catalysis (York and O'Neill, 2008; Liwanag et al., 2012; Jensen et al., 2014; Urbanowicz et al., 2014). This is in contrast with processive enzymes, such as cellulose synthase, where the product remains associated with the enzyme. Biosynthesis of β-(1,4)-xylan (this study) and β-(1,4)-galactan (Rautengarten et al., 2014) have been found to be affected by specific nucleotide transporters, and we speculate that the functional association with a transporter is a mechanism that allows the synthases to maintain a degree of processivity and operate efficiently in vivo.

In mammalian cells, UXS enzymes are located only in the Golgi lumen and UDP-Xyl transport is therefore apparently not required (Ashikov et al., 2005). However, a mutant in the UXS enzyme in Chinese hamster ovary cells could be complemented by a cytoplasmic isoform of UXS from Arabidopsis, showing that in these cells the route for delivery of UDP-Xyl is not important for the function of the xylosyltransferases (Bakker et al., 2009). Since UDP-Xyl in plants is biosynthesized both in the cytoplasm and in the Golgi lumen by UXS enzymes, it seemed highly likely that plant UDP-Xyl transport into the Golgi would be a redundant process. However, our results show that, at least for xylan biosynthesis, the transport of UDP-Xyl is important and the Golgi-localized UXS enzymes cannot deliver sufficient UDP-Xyl for proper xylan biosynthesis.

Conclusions

We identified three Golgi-localized nucleotide sugar transporters that are able to transport UDP-Xyl in vitro. This demonstrates the existence of NSTs with specificity for UDP-Xyl in plants. *uxt1* mutant plants showed a significant decrease in total cell wall Xyl content in stems, thus confirming a role for UXT1 in providing UDP-Xyl for cell wall biosynthesis.

METHODS

Nucleotide and Nucleotide Sugar Standards

Nucleotide and nucleotide sugar standards were obtained from the following sources: UDP-α-D-xylose, UDP-β-L-arabinopyranose, and UDP-α-D-galacturonic acid (Carbosource Services, Complex Carbohydrate Research Center, Athens, GA); UMP, GMP, CMP, AMP, UDP-α-D-glucuronic acid, UDP-α-D-glucose, UDP-α-D-galactose, UDP-*N*-acetyl-α-D-glucosamine, UDP-*N*-acetyl-α-D-galactosamine, GDP-α-D-mannose, GDP-β-L-fucose, GDP-α-D-glucose, adenosine 3′-phosphate 5′ phosphosulfate, CMP-*N*-acetylneuraminic acid, and ADP-α-D-glucose (Sigma-Aldrich); and UDP-β-L-arabinofuranose (Peptides International). GDP-α-L-galactose

was enzymatically synthesized according to Major et al. (2005) and HPLC purified using a linear ammonium formate gradient (Rautengarten et al., 2011). UDP-β-L-rhamnose was enzymatically synthesized by a two-step reaction using UDP-Glc as substrate as previously described (Rautengarten et al., 2014).

Sequence Analysis

Amino acid sequences were retrieved from The Arabidopsis Information Resource (Lamesch et al., 2012). Deduced amino acid sequences were aligned using the Clustal Omega program (Sievers et al., 2011) using default parameters (Supplemental Data Set 1). Phylogenetic trees were created using the neighbor-joining statistical method and applying the bootstrap method with 1000 replications and visualized using the Molecular Evolutionary Genetics Analysis (MEGA) version 6.0 application (Tamura et al., 2013).

Heterologous Expression, Reconstitution, and in Vitro Assay of Transport Activities

Heterologous expression in *Saccharomyces cerevisiae* (strain INVSc1: *MATa his3D1 leu2 trp1-289 ura3-52 MAT his3D1 leu2 trp1-289 ura3-52*; Life Technologies), reconstitution of microsomal proteins, and subsequent transport activity assay were performed as previously described (Rautengarten et al., 2014). Kinetic parameters were calculated by nonlinear regression using the Prism6 application (GraphPad Software). PAGE and immunoblot analyses were done as previously described (Rautengarten et al., 2011) using 2.5 μg yeast microsomal protein. Filters were probed using the anti-V5 antibody (Life Technologies).

Chromatographic Separation and Detection of Nucleotide Sugars by Mass Spectrometry

LC-MS/MS was performed using porous graphitic carbon as the stationary phase on an 1100 series HPLC system (Agilent Technologies) and a 4000 QTRAP LC-MS/MS system (AB Sciex) equipped with a TurboIonSpray ion source using methods previously described (Ito et al., 2014; Rautengarten et al., 2014)

Absolute Quantification of Reconstituted NSTs by MRM Mass Spectrometry

The yeast expression vector pYES-DEST52 contains an in-frame V5-tag and 6xHis-tag epitope at the 3′ end of the cloning site. The expressed UXT proteins all yield a common tryptic peptide, namely, R.SRGPFEGK-PIPNPLLGLDSTR.T, as previously described (Rautengarten et al., 2014). A synthesized peptide was used to determine optimal parameters for MRM analysis with the following parameters: dwell (25 ms), fragmentor (130 V), collision energy (11.1 V), and cell accelerator voltage (7 V). Analysis of samples and standard curves were conducted on a 6460 Triple Quad LC/MS system equipped with a Jet Stream ESI source (Agilent Technologies). The system was operated in positive ion mode using the MRM scan type with both MS1 and MS2 resolutions set to unit. The following mass spectrometer parameters were applied: gas temperature (350°C), gas flow (10 L/min), nebulizer (45 p.s.i.), sheath gas temperature (400°C), sheath gas flow (11 L/min), capillary (5000 V), and MS1/MS2 heater (100°C). A total of 5 μg of trypsin-digested (1:10 [w/w]) proteoliposome was loaded onto an Ascentis Express Peptide ES-C18 (5 cm × 2.1 mm, 2.7 μm) column (Sigma-Aldrich) using a 1290 series HPLC (Agilent Technologies) at a flow rate of 0.4 mL/min as follows: 95% Buffer A (99.9% water and 0.1% formic acid) and 5% Buffer B (99.9% acetonitrile and 0.1% formic acid) for 0.2 min, followed by an increase to 35% Buffer B over 5.5 min, then 90% Buffer B in 0.3 min, where it was held for 2 min. The buffer composition was ramped back to 5% Buffer B over 5 min, giving a total runtime of 13 min. The column temperature was maintained at 60°C. Data were acquired using MassHunter Workstation Software Version B.06.00 Build 6.0.6025.4 SP4 (Agilent Technologies). The raw data were imported into Skyline (v2.5.0.6157) (MacLean et al., 2010) and transition peaks manually inspected for retention time and adjusted accordingly. The abundance of the expressed UXTs in a sample was calculated by integrating the total signal peak area (total area) from Skyline for the two transitions on the predominant 563.560 $[M+4H]^{4+}$ precursor ion, namely, L [*y*7] 761.452 $[M+H]^{1+}$ and G [*y*6] 648.3311 $[M+H]^{1+}$, and calculating total moles in the sample against a standard curve for the synthesized peptide. The standard curve was created by linear regression using a range of abundances (0.5 to 10 pmol), which were interspersed as separate runs during sample analysis. The UXTs represent from 0.01 to 0.1% of total protein of the reconstituted proteoliposomes with errors representing the SD of two technical replicates (Supplemental Table 1). Values were used for enzyme kinetic calculations.

Plant Material and Growth Conditions

Arabidopsis thaliana Col-0 was obtained from the ABRC (http://abrc.osu.edu/). T-DNA insertion mutants for *UXT1* (*uxt1-1*, SAIL_147_F11; *uxt1-2*, SALK_086773), *UXT2* (*uxt2-1*, SALK_078576), and *UXT3* (*uxt3-1*, SALK_013372) were obtained from the SIGnAL Salk collection (http://signal.salk.edu/). Plants were germinated and grown on soil (PRO-MIX; Premier Horticulture) in an Arabidopsis growth chamber (Percival-Scientific) under short-day light conditions (10 h of fluorescent light [120 μmol m^{-2} s^{-1}] at 22°C and 60% RH/14 h of dark at 22°C and 60% RH). After 4 weeks, plants were transferred to long-day conditions (16 h of fluorescent light [120 μmol m^{-2} s^{-1}] at 22°C and 60% RH/8 h of dark at 22°C and 60% RH).

Cloning Procedures

Coding sequences for Arabidopsis UXTs without native stop codon were PCR amplified using the primer pairs listed in Supplemental Table 3. PCR products were introduced into the pENTR/SD/D-TOPO cloning vector (Life Technologies) according to the manufacturer's protocol and confirmed by sequencing. To obtain C-terminal YFP fusions, the constructs were introduced into the 35S promoter carrying pEarleyGate101 plant transformation vector (Earley et al., 2006) using the LR Clonase II reaction (Life Technologies) following the manufacturer's protocol. For yeast expression, the constructs were introduced into the yeast expression vector pYES-DEST52 (Life Technologies) using the LR Clonase II reaction (Life Technologies).

Subcellular Localization and Microscopy

Nicotiana benthamiana plants were grown on soil (PRO-MIX) in a growth chamber (Percival-Scientific) using the following conditions: 24°C day/night temperature, 60% humidity, and 16-h-light/8-h-dark cycles. Four-week-old leaves were coinfiltrated with *Agrobacterium tumefaciens* strain GV3101 pmp90 carrying the C-terminal YFP fusion constructs (OD_{600} = 0.15) and the α-mannosidase-mCherry marker (OD_{600} = 0.01) (Nelson et al., 2007) using the previously described method (Jensen et al., 2008). Visualization by confocal laser scanning microscopy was performed as previously described (Rautengarten et al., 2012).

Determination of Monosaccharide Composition

AIR was prepared as described earlier (Harholt et al., 2006). Samples were hydrolyzed in 2 N trifluoroacetic acid for 1 h at 120°C. HPAEC with pulsed amperometric detection was performed as described (ØBro et al., 2004) on an ICS 3000 (Dionex) using a CarboPac PA20 anion exchange column (3 × 150 mm; Dionex).

PCR Characterization of Mutants

Homozygous T-DNA insertion lines were verified by PCR to confirm the presence of the insert using the primers listed in Supplemental Table 3. Subsequently, absence of the transcript was verified by RT-PCR using the primers listed in Supplemental Table 3. Arabidopsis *ACTIN-2* (At3g18780) was used as a control for equal loading.

RT-PCR

Plant RNA was extracted using the RNEasy RNA Plant Kit (Qiagen) according to the manufacturer's protocol, and 0.5 to 1 μg was reverse transcribed using SuperScript II reverse transcriptase and $d(T)_{15}$ oligomers (Life Technologies) according to the manufacturer's protocol. *UXT1-3* expression in different organs was analyzed by quantitative RT-PCR using SYBR Select Master Mix (Applied Biosystems) on a StepOnePlus Real-Time PCR system (Applied Biosystems) according to the conditions described earlier (Czechowski et al., 2005) using StepOne 2.0 software (Applied Biosystems). The *UXT* genes were amplified using the primers listed in Supplemental Table 3. As references, primers for *UBQ10* (At4g05320), *PP2A* (At1g13320), and a *SAND* family member (*MON1*, At2g28390) were used (Supplemental Table 3). Expression levels were calculated using the comparative CT method, which involves normalizing against the geometric mean of the three housekeeping genes (*UBI10*, *PP2A* and *SAND* family) for each tissue type (Schmittgen and Livak, 2008).

Xylan Oligosaccharide Profiling

Xylan was digested with endoglucuronoxylanase GH30 (XynC) from *Bacillus subtilis* (St John et al., 2006) as previously described (Bromley et al., 2013). Profiling of the released oligosaccharides by HPAEC was performed using the conditions previously described (Chiniquy et al., 2012). Cell wall preparations from the *gux1* and *gux2* mutants (Oikawa et al., 2010; Bromley et al., 2013) were analyzed for comparison.

Protein Extraction and Immunoblotting

Inflorescence stems from 6-week-old plants were ground in extraction buffer (10 mM Tris, pH 8, 150 mM NaCl, 2% Triton, 1 mM PMSF, protease inhibitor, and 10 mM $CaCl_2$) incubated for 1 h at 4°C under constant shaking, and centrifuged for 30 min at 20,800*g* at 4°C to remove cell debris. Subsequently, protein was precipitated with 20% trichloroacetic acid, incubated on ice, and spun down. After removal of the supernatant, the samples were washed twice with ice-cold acetone, dried, and suspended in the appropriate buffer. Samples were separated by SDS-PAGE, and glycosylation was detected by immunoblotting using antibodies raised against β-(1,2)-Xyl and α-(1,3)-Fuc (Agrisera). Detection was performed with an ECL Plus Western Blotting Detection System (GE Healthcare).

OLIMP

Mass profiling of xyloglucan oligosaccharides derived from various stem tissues was performed as previously described (Lerouxel et al., 2002). The cell wall material was digested with a xyloglucans-specific endoglucanase (Pauly et al., 1999), and the resulting solubilized xyloglucan oligosaccharides were detected using an Axima matrix-assisted laser desorption/ionization time-of-flight system (Shimadzu) set in linear positive mode with an acceleration voltage of 20,000 V.

CoMPP

CoMPP was undertaken essentially according to previously described work (Moller et al., 2007). AIR samples were extracted from mature stems of pooled material (approximately eight individuals) from 8-week-old *uxt1-1*, *uxt1-2*, and wild-type plants. A total of 4 mg AIR was subsequently extracted sequentially with CDTA and then NaOH solutions to obtain pectin-rich and hemicellulose-rich extracts, respectively. These extracts were spotted onto membranes and probed with monoclonal antibodies and carbohydrate binding modules (CBMs) that recognize specific cell wall epitopes, namely, LM3, extensins; LM25, xyloglucan; LM10, β-(1-4)-D-xylan; LM11, (1-4)-β-D-xylan; UX1, glucuronoxylan; AX1, arabinose substituted β-(1-4)-D-xylan; and CBM3a, cellulose (Guillon et al., 2004; McCartney et al., 2005; Blake et al., 2006; Koutaniemi et al., 2012; Pedersen et al., 2012).

Accession Numbers

Sequence data from this article can be found in the Arabidopsis Genome Initiative or GenBank/EMBL databases under the following accession numbers: *UXT1* (AT2G28315), *UXT2* (AT2G30460), *UXT3* (AT1G06890), *ACTIN-2* (At3g18780), *UBQ10* (At4g05320), *PP2A* (At1g13320), and *MON1* (At2g28390).

Supplemental Data

Supplemental Figure 1. Subcellular localization of *UXT1* with an ER marker.

Supplemental Figure 2. Assessment of *UXT* transcripts by RT-PCR in the of *uxt* mutant backgrounds.

Supplemental Figure 3. The 4-*O*-Methyl-D-glucuronic acid content of pooled stem material.

Supplemental Figure 4. Xylan profiling of the *uxt1* mutants.

Supplemental Figure 5. Immunoblot analysis of *N*-glycosylation in the *uxt* mutants.

Supplemental Table 1. Calculations of UXT protein contents in reconstituted proteoliposomes used for transport assays.

Supplemental Table 2. Monosaccharide composition of *UXT* mutant cell wall preparations derived from different Arabidopsis organs.

Supplemental Table 3. Primer list.

Supplemental Data Set 1. Text file of the alignment used for the phylogenetic analysis shown in Figure 1.

ACKNOWLEDGMENTS

This work was supported by the U. S. Department of Energy, Office of Science, Office of Biological and Environmental Research, through Contract DE-AC02-05CH11231 between the Lawrence Berkeley National Laboratory and the U.S. Department of Energy. J.L.H. is supported by an Australian Research Council Future Fellowship (FT130101165). Part of the work was supported by the Danish Strategic Research Council (Set4Future 11-116795). The substrates obtained from Carbosource Services (Athens, GA) were supported in part by NSF-RCN Grant 0090281. We thank James F. Preston (University of Florida) for the generous gift of xylanase XynC and Breeanna Urbanowicz (University of Georgia) for providing a 4-*O*-Me-GlcA standard. We also thank Devon Birdseye and Mi Yeon Lee for assistance with plant growth and maintenance.

AUTHOR CONTRIBUTIONS

B.E., C.R., P.D.A., C.J.P., J.L.H., and H.V.S. designed the study and directed its implementation. B.E., C.R., X.G., G.X., T.H., L.J.G.C., and S.S. conducted the experiments. B.E., C.R., J.L.H., A.M.S.-M., M.P., W.G.T.W., and H.V.S. analyzed the data. B.E., C.R., J.L.H., and H.V.S. wrote the article.

Received October 29, 2014; revised February 19, 2015; accepted March 5, 2015; published March 24, 2015.

REFERENCES

Ashikov, A., Routier, F., Fuhlrott, J., Helmus, Y., Wild, M., Gerardy-Schahn, R., and Bakker, H. (2005). The human solute carrier gene SLC35B4 encodes a bifunctional nucleotide sugar transporter with specificity for UDP-xylose and UDP-*N*-acetylglucosamine. J. Biol. Chem. **280:** 27230–27235.

Atmodjo, M.A., Hao, Z., and Mohnen, D. (2013). Evolving views of pectin biosynthesis. Annu. Rev. Plant Biol. **64:** 747–779.

Bakker, H., Routier, F., Ashikov, A., Neumann, D., Bosch, D., and Gerardy-Schahn, R. (2008). A CMP-sialic acid transporter cloned from *Arabidopsis thaliana.* Carbohydr. Res. **343:** 2148–2152.

Bakker, H., Routier, F., Oelmann, S., Jordi, W., Lommen, A., Gerardy-Schahn, R., and Bosch, D. (2005). Molecular cloning of two Arabidopsis UDP-galactose transporters by complementation of a deficient Chinese hamster ovary cell line. Glycobiology **15:** 193–201.

Bakker, H., Oka, T., Ashikov, A., Yadav, A., Berger, M., Rana, N.A., Bai, X., Jigami, Y., Haltiwanger, R.S., Esko, J.D., and Gerardy-Schahn, R. (2009). Functional UDP-xylose transport across the endoplasmic reticulum/Golgi membrane in a Chinese hamster ovary cell mutant defective in UDP-xylose Synthase. J. Biol. Chem. **284:** 2576–2583.

Baldwin, T.C., Handford, M.G., Yuseff, M.I., Orellana, A., and Dupree, P. (2001). Identification and characterization of GONST1, a Golgi-localized GDP-mannose transporter in Arabidopsis. Plant Cell **13:** 2283–2295.

Bar-Peled, M., and O'Neill, M.A. (2011). Plant nucleotide sugar formation, interconversion, and salvage by sugar recycling. Annu. Rev. Plant Biol. **62:** 127–155.

Blake, A.W., McCartney, L., Flint, J.E., Bolam, D.N., Boraston, A.B., Gilbert, H.J., and Knox, J.P. (2006). Understanding the biological rationale for the diversity of cellulose-directed carbohydrate-binding modules in prokaryotic enzymes. J. Biol. Chem. **281:** 29321–29329.

Bromley, J.R., Busse-Wicher, M., Tryfona, T., Mortimer, J.C., Zhang, Z., Brown, D.M., and Dupree, P. (2013). GUX1 and GUX2 glucuronyltransferases decorate distinct domains of glucuronoxylan with different substitution patterns. Plant J. **74:** 423–434.

Chiniquy, D., et al. (2012). XAX1 from glycosyltransferase family 61 mediates xylosyltransfer to rice xylan. Proc. Natl. Acad. Sci. USA **109:** 17117–17122.

Czechowski, T., Stitt, M., Altmann, T., Udvardi, M.K., and Scheible, W.R. (2005). Genome-wide identification and testing of superior reference genes for transcript normalization in Arabidopsis. Plant Physiol. **139:** 5–17.

Earley, K.W., Haag, J.R., Pontes, O., Opper, K., Juehne, T., Song, K., and Pikaard, C.S. (2006). Gateway-compatible vectors for plant functional genomics and proteomics. Plant J. **45:** 616–629.

Ebringerová, A., and Heinze, T. (2000). Xylan and xylan derivatives: biopolymers with valuable properties, 1 Naturally occurring xylans structures, procedures and properties. Macromol. Rapid Commun. **21:** 542–556.

Egelund, J., Petersen, B.L., Motawia, M.S., Damager, I., Faik, A., Olsen, C.E., Ishii, T., Clausen, H., Ulvskov, P., and Geshi, N. (2006). *Arabidopsis thaliana* RGXT1 and RGXT2 encode Golgi-localized (1,3)-alpha-D-xylosyltransferases involved in the synthesis of pectic rhamnogalacturonan-II. Plant Cell **18:** 2593–2607.

Fitchette-Lainé, A.C., Gomord, V., Chekkafi, A., and Faye, L. (1994). Distribution of xylosylation and fucosylation in the plant Golgi-apparatus. Plant J. **5:** 673–682.

Fry, S.C., et al. (1993). An unambiguous nomenclature for xyloglucan-derived oligosaccharides. Physiol. Plant. **89:** 1–3.

Guillon, F., Tranquet, O., Quillien, L., Utille, J.P., Ortiz, J.J.O., and Saulnier, L. (2004). Generation of polyclonal and monoclonal antibodies against arabinoxylans and their use for immunocytochemical location of arabinoxylans in cell walls of endosperm of wheat. J. Cereal Sci. **40:** 167–182.

Handford, M., Rodríguez-Furlán, C., Marchant, L., Segura, M., Gómez, D., Alvarez-Buylla, E., Xiong, G.Y., Pauly, M., and Orellana, A. (2012). *Arabidopsis thaliana* AtUTr7 encodes a golgi-localized UDP-glucose/UDP-galactose transporter that affects lateral root emergence. Mol. Plant **5:** 1263–1280.

Handford, M.G., Sicilia, F., Brandizzi, F., Chung, J.H., and Dupree, P. (2004). *Arabidopsis thaliana* expresses multiple Golgi-localised nucleotide-sugar transporters related to GONST1. Mol. Genet. Genomics **272:** 397–410.

Harholt, J., Jensen, J.K., Sørensen, S.O., Orfila, C., Pauly, M., and Scheller, H.V. (2006). ARABINAN DEFICIENT 1 is a putative arabinosyltransferase involved in biosynthesis of pectic arabinan in Arabidopsis. Plant Physiol. **140:** 49–58.

Harper, A.D., and Bar-Peled, M. (2002). Biosynthesis of UDP-xylose. Cloning and characterization of a novel Arabidopsis gene family, UXS, encoding soluble and putative membrane-bound UDP-glucuronic acid decarboxylase isoforms. Plant Physiol. **130:** 2188–2198.

Ito, J., Herter, T., Baidoo, E.E., Lao, J., Vega-Sánchez, M.E., Michelle Smith-Moritz, A., Adams, P.D., Keasling, J.D., Usadel, B., Petzold, C.J., and Heazlewood, J.L. (2014). Analysis of plant nucleotide sugars by hydrophilic interaction liquid chromatography and tandem mass spectrometry. Anal. Biochem. **448:** 14–22.

Jensen, J.K., Johnson, N.R., and Wilkerson, C.G. (2014). *Arabidopsis thaliana* IRX10 and two related proteins from psyllium and *Physcomitrella patens* are xylan xylosyltransferases. Plant J. **80:** 207–215.

Jensen, J.K., et al. (2008). Identification of a xylogalacturonan xylosyltransferase involved in pectin biosynthesis in Arabidopsis. Plant Cell **20:** 1289–1302.

Knappe, S., Flügge, U.I., and Fischer, K. (2003). Analysis of the plastidic phosphate translocator gene family in Arabidopsis and identification of new phosphate translocator-homologous transporters, classified by their putative substrate-binding site. Plant Physiol. **131:** 1178–1190.

Koutaniemi, S., Guillon, F., Tranquet, O., Bouchet, B., Tuomainen, P., Virkki, L., Petersen, H.L., Willats, W.G., Saulnier, L., and Tenkanen, M. (2012). Substituent-specific antibody against glucuronoxylan reveals close association of glucuronic acid and acetyl substituents and distinct labeling patterns in tree species. Planta **236:** 739–751.

Lamesch, P., et al. (2012). The Arabidopsis Information Resource (TAIR): improved gene annotation and new tools. Nucleic Acids Res. **40:** D1202–D1210.

Lerouxel, O., Choo, T.S., Séveno, M., Usadel, B., Faye, L., Lerouge, P., and Pauly, M. (2002). Rapid structural phenotyping of plant cell wall mutants by enzymatic oligosaccharide fingerprinting. Plant Physiol. **130:** 1754–1763.

Liepman, A.H., Wightman, R., Geshi, N., Turner, S.R., and Scheller, H.V. (2010). Arabidopsis - a powerful model system for plant cell wall research. Plant J. **61:** 1107–1121.

Liwanag, A.J., Ebert, B., Verhertbruggen, Y., Rennie, E.A., Rautengarten, C., Oikawa, A., Andersen, M.C., Clausen, M.H., and Scheller, H.V. (2012). Pectin biosynthesis: GALS1 in *Arabidopsis thaliana* is a β-1,4-galactan β-1,4-galactosyltransferase. Plant Cell **24:** 5024–5036.

MacLean, B., Tomazela, D.M., Shulman, N., Chambers, M., Finney, G.L., Frewen, B., Kern, R., Tabb, D.L., Liebler, D.C., and MacCoss, M.J. (2010). Skyline: an open source document editor for creating and analyzing targeted proteomics experiments. Bioinformatics **26:** 966–968.

Major, L.L., Wolucka, B.A., and Naismith, J.H. (2005). Structure and function of GDP-mannose-3′,5′-epimerase: an enzyme which performs three chemical reactions at the same active site. J. Am. Chem. Soc. **127:** 18309–18320.

McCartney, L., Marcus, S.E., and Knox, J.P. (2005). Monoclonal antibodies to plant cell wall xylans and arabinoxylans. J. Histochem. Cytochem. **53:** 543–546.

Mølhøj, M., Verma, R., and Reiter, W.D. (2003). The biosynthesis of the branched-chain sugar d-apiose in plants: functional cloning and characterization of a UDP-d-apiose/UDP-d-xylose synthase from Arabidopsis. Plant J. **35:** 693–703.

Moller, I., Sørensen, I., Bernal, A.J., Blaukopf, C., Lee, K., Øbro, J., Pettolino, F., Roberts, A., Mikkelsen, J.D., Knox, J.P., Bacic, A., and Willats, W.G. (2007). High-throughput mapping of cell-wall polymers within and between plants using novel microarrays. Plant J. **50:** 1118–1128.

Mortimer, J.C., et al. (2013). Abnormal glycosphingolipid mannosylation triggers salicylic acid-mediated responses in Arabidopsis. Plant Cell **25:** 1881–1894.

Nelson, B.K., Cai, X., and Nebenführ, A. (2007). A multicolored set of *in vivo* organelle markers for co-localization studies in Arabidopsis and other plants. Plant J. **51:** 1126–1136.

Norambuena, L., Marchant, L., Berninsone, P., Hirschberg, C.B., Silva, H., and Orellana, A. (2002). Transport of UDP-galactose in plants. Identification and functional characterization of AtUTr1, an *Arabidopsis thaliana* UDP-galactos/UDP-glucose transporter. J. Biol. Chem. **277:** 32923–32929.

Norambuena, L., Nilo, R., Handford, M., Reyes, F., Marchant, L., Meisel, L., and Orellana, A. (2005). AtUTr2 is an *Arabidopsis thaliana* nucleotide sugar transporter located in the Golgi apparatus capable of transporting UDP-galactose. Planta **222:** 521–529.

ØBro, J., Harholt, J., Scheller, H.V., and Orfila, C. (2004). Rhamnogalacturonan I in *Solanum tuberosum* tubers contains complex arabinogalactan structures. Phytochemistry **65:** 1429–1438.

Oikawa, A., Joshi, H.J., Rennie, E.A., Ebert, B., Manisseri, C., Heazlewood, J.L., and Scheller, H.V. (2010). An integrative approach to the identification of Arabidopsis and rice genes involved in xylan and secondary wall development. PLoS ONE **5:** e15481.

Pattathil, S., Harper, A.D., and Bar-Peled, M. (2005). Biosynthesis of UDP-xylose: characterization of membrane-bound *AtUxs2.* Planta **221:** 538–548.

Pauly, M., Andersen, L.N., Kauppinen, S., Kofod, L.V., York, W.S., Albersheim, P., and Darvill, A. (1999). A xyloglucan-specific *endo*-β-1,4-glucanase from *Aspergillus aculeatus*: expression cloning in yeast, purification and characterization of the recombinant enzyme. Glycobiology **9:** 93–100.

Pedersen, H.L., et al. (2012). Versatile high resolution oligosaccharide microarrays for plant glycobiology and cell wall research. J. Biol. Chem. **287:** 39429–39438.

Rautengarten, C., Ebert, B., Herter, T., Petzold, C.J., Ishii, T., Mukhopadhyay, A., Usadel, B., and Scheller, H.V. (2011). The interconversion of UDP-arabinopyranose and UDP-arabinofuranose is indispensable for plant development in Arabidopsis. Plant Cell **23:** 1373–1390.

Rautengarten, C., Ebert, B., Ouellet, M., Nafisi, M., Baidoo, E.E., Benke, P., Stranne, M., Mukhopadhyay, A., Keasling, J.D., Sakuragi, Y., and Scheller, H.V. (2012). Arabidopsis Deficient in Cutin Ferulate encodes a transferase required for feruloylation of ω-hydroxy fatty acids in cutin polyester. Plant Physiol. **158:** 654–665.

Rautengarten, C., et al. (2014). The Golgi localized bifunctional UDP-rhamnose/UDP-galactose transporter family of Arabidopsis. Proc. Natl. Acad. Sci. USA **111:** 11563–11568.

Rennie, E.A., and Scheller, H.V. (2014). Xylan biosynthesis. Curr. Opin. Biotechnol. **26:** 100–107.

Rollwitz, I., Santaella, M., Hille, D., Flügge, U.I., and Fischer, K. (2006). Characterization of AtNST-KT1, a novel UDP-galactose transporter from *Arabidopsis thaliana.* FEBS Lett. **580:** 4246–4251.

Scheible, W.R., and Pauly, M. (2004). Glycosyltransferases and cell wall biosynthesis: novel players and insights. Curr. Opin. Plant Biol. **7:** 285–295.

Scheller, H.V., and Ulvskov, P. (2010). Hemicelluloses. Annu. Rev. Plant Biol. **61:** 263–289.

Schmid, M., Davison, T.S., Henz, S.R., Pape, U.J., Demar, M., Vingron, M., Schölkopf, B., Weigel, D., and Lohmann, J.U. (2005). A gene expression map of *Arabidopsis thaliana* development. Nat. Genet. **37:** 501–506.

Schmittgen, T.D., and Livak, K.J. (2008). Analyzing real-time PCR data by the comparative C(T) method. Nat. Protoc. **3:** 1101–1108.

Sievers, F., Wilm, A., Dineen, D., Gibson, T.J., Karplus, K., Li, W., Lopez, R., McWilliam, H., Remmert, M., Söding, J., Thompson, J.D., and Higgins, D.G. (2011). Fast, scalable generation of high-quality protein multiple sequence alignments using Clustal Omega. Mol. Syst. Biol. **7:** 539.

St John, F.J., Rice, J.D., and Preston, J.F. (2006). Characterization of XynC from *Bacillus subtilis* subsp. *subtilis* strain 168 and analysis of its role in depolymerization of glucuronoxylan. J. Bacteriol. **188:** 8617–8626.

Strasser, R., Mucha, J., Mach, L., Altmann, F., Wilson, I.B., Glössl, J., and Steinkellner, H. (2000). Molecular cloning and functional expression of β1, 2-xylosyltransferase cDNA from *Arabidopsis thaliana.* FEBS Lett. **472:** 105–108.

Tamura, K., Stecher, G., Peterson, D., Filipski, A., and Kumar, S. (2013). MEGA6: Molecular Evolutionary Genetics Analysis version 6.0. Mol. Biol. Evol. **30:** 2725–2729.

Tan, L., et al. (2013). An Arabidopsis cell wall proteoglycan consists of pectin and arabinoxylan covalently linked to an arabinogalactan protein. Plant Cell **25:** 270–287.

Urbanowicz, B.R., Peña, M.J., Moniz, H.A., Moremen, K.W., and York, W.S. (2014). Two Arabidopsis proteins synthesize acetylated xylan *in vitro.* Plant J. **80:** 197–206.

York, W.S., and O'Neill, M.A. (2008). Biochemical control of xylan biosynthesis - which end is up? Curr. Opin. Plant Biol. **11:** 258–265.

Zhang, B., Liu, X., Qian, Q., Liu, L., Dong, G., Xiong, G., Zeng, D., and Zhou, Y. (2011). Golgi nucleotide sugar transporter modulates cell wall biosynthesis and plant growth in rice. Proc. Natl. Acad. Sci. USA **108:** 5110–5115.